

Effects of magma-induced stress within a cellular automaton model of volcanism

Olivia J. Butters^a, Graeme R. Sarson^{a,*}, Paul J. Bushby^a

^a*School of Mathematics & Statistics, Newcastle University, Newcastle upon Tyne NE1 7RU, UK*

Abstract

The cellular automaton model of Piegari, Di Maio, Scandone and Milano, *J. Volc. Geoth. Res.*, **202**, 22-28 (2011) is extended to include magma-induced stress (i.e. a local magma-related augmentation of the stress field). This constitutes a nonlinear coupling between the magma and stress fields considered by this model, which affects the statistical distributions of eruptions obtained. The extended model retains a power law relation between eruption size and frequency for most events, as expected from the self-organised criticality inspiring this model; but the power law now applies for a reduced range of size, and there are new peaks of relatively more frequent eruptions of intermediate and large size. The cumulative frequency of repose time between events remains well modelled by a stretched exponential function of repose time (approaching a pure exponential distribution only for the longest repose times), but the time scales of this behaviour are slightly longer, reflecting the increased preference for larger events. The eruptions are relatively more likely to have high volatile (water) content, so would generally be more explosive. The new model also naturally favours a central ‘axial’ transport conduit, as found in many volcano systems, but which otherwise must be artificially imposed within such models.

Keywords: magma ascent, cellular automaton, self-organised criticality, volcanism

1. Introduction

Volcanism occurs in a variety of styles, ranging from effusive to explosive, with orders of magnitude variation in the volume of ejecta and in the repose time between eruptions. This reflects the wide range of tectonic settings, magma compositions, and variations in structure of the volcanic conduit(s) through which magma is transported (Newhall, 2007; Siebert et al., 2010). Despite these variations between different systems, some statistical features of eruptions are well-established. Quantifying the magnitude of an eruption using the Volcanic Explosivity Index, VEI (Newhall and Self, 1982), Simkin (1993) demonstrated an exponential relation between the frequency of Holocene eruptions and their magnitude, for VEI values in the range 2–7. This corresponds to a power law relation between eruption frequency and the volume of ejecta, since a unit increase in VEI corresponds to a factor of 10 increase in ejecta. This power law relation can be compared to the well-known Gutenberg–Richter law for earthquakes (Gutenberg and Richter, 1956), with VEI playing a similar role to the earthquake magnitude M . Indeed, many parallels can be drawn between volcanic activity and tectonic activity on fault zones (Newhall, 2007).

Power law behaviour is often a signature of Self-Organised Criticality, SOC (e.g. Jensen, 1998). Ideas of self-organisation in volcano fracture systems go back at least to Shaw and Chouet (1991), who considered fractal percolation networks beneath Hawaiian volcanoes, and the nonlinear dynamics linking these to tremor processes. Additional support for SOC in volcanism

comes from the ‘pink’ (i.e. self-similar, $1/f$) spectrum of noise observed in long period volcanic seismicity (Lachowycz et al., 2013). Such a spectrum is often associated with SOC processes.

Cellular automata (CA) often exhibit SOC, and such systems have long been used to model seismicity. Bak and Tang (1989) extended their original sandpile model (Bak et al., 1988) to consider earthquakes, and noted the connection with the Gutenberg–Richter law. Olami, Feder and Christensen (1992; OFC) made such CA models non-conservative, to allow for the energy loss in seismic motion, and the OFC earthquake model has become one of the ‘standard’ SOC systems (e.g. Jensen, 1998). The OFC model is an abstract representation of the ‘slider block’ model of seismicity (Burridge and Knopoff, 1967), with the equations of motion of the spring blocks being replaced by a CA consisting of a grid of cells on which the associated stress distribution evolves according to a simple set of rules (e.g. Turcotte, 1997).

The 2D OFC model is normally assumed to represent an abstract section of a fault plane subject to a constant applied stress; the earthquake events arise from local ‘stick-slip’ behaviour, which might remain localised (small events) or trigger an ‘avalanche’ of events involving neighbouring cells (leading to larger events). Piegari et al. (2008) instead applied the model to a vertical section of crust below a volcano, with the constant rate of stress representing a combination of the regional stress field and the local stresses associated with the volcanism. To this they added a linked CA model, representing the presence of magma within the volcano, with rules for the feeding of the system from an underlying reservoir, for the movement of magma under buoyancy, and for the eruption of magma as lava at the surface. Within this model, magma movement is

*Corresponding author.

Email address: g.r.sarson@newcastle.ac.uk (Graeme R. Sarson)

only allowed within the network of fractured cells created by earthquake events; this model therefore embodies the ‘magma batch’ mechanism advanced by Scandone et al. (2007), appropriate for closed conduit volcanoes, and presented as a model for the late 20th century activity of Mount St Helens (1980–2004) and Pinatubo (1991).

The original model of Piegari et al. (2008) was extended in subsequent papers, to model the volatile components within the magma (Piegari et al., 2011), and to investigate different background density profiles (Piegari et al., 2012) and the effect of a low-density surface layer (Piegari et al., 2013); some of the details of these models are presented and discussed in sections 2 and 4. While these models are highly idealised, they produce eruptions ranging greatly in size (i.e. the number of cells of magma involved in the eruption), with the expected power law relation between frequency and size holding across most of the range. The system thus appears to be a useful working model for the style of volcanism described by Scandone et al. (2007).

While the papers of Piegari et al. usefully extend the CA model of earthquakes to volcanism, they do not allow for any feedback from the magma activity upon the local seismicity (potentially an important effect within linked seismic-volcanic systems). Many studies corroborate the association between seismicity and magma activity. The occurrence of volcano-tectonic (VT) events — ‘normal’ tectonic earthquakes due to brittle fracture (shear failure), swarms of which may occur as precursors of eruptions — is often explained via changes in the stress field directly caused by the rising magma, and by later relaxation (e.g. Newhall, 2007). The fracturing of the country rock by a propagating crack of buoyant magma has often been studied as a fluid mechanical problem (e.g. Emerman et al., 1986; Lister and Kerr, 1991). Kilburn and Voight (1998) note that direct magmatic stresses need not be the only effect, and propose a model for subcritical rock failure due to progressive weakening, most likely due to stress corrosion: a stress-enhanced chemical reaction due to circulating fluids. Such circulation may nevertheless also be associated with nearby magma intrusion. VT events contrast with long-period (LP; low-frequency) events associated with the degassing of magma at shallow depths, and with dome formation (Neuberg, 2000). Non-explosive magma fragmentation, due to degassing, may also lead to the creation of intermittent fracture networks near the magma conduits (Gonnermann and Manga, 2003).

Although different in nature, both VT and LP events could be modelled within the CA system by feedback from the magma field to earthquake events. We do not propose any specific mechanism for magma-induced stress, but instead (in the idealised spirit of the CA model) simply introduce a local enhancement of the strain rate in the vicinity of magma, as described in detail in section 2. As a final comment, we note that Scandone et al. (2007) suggest that the complexity of the fracture system may systematically increase with time during episodes of volcanism; this possibility is absent from the models of Piegari et al. (where the stress field is independent of the magma), but not for our model (where increased magma in the system will naturally lead to more widespread fracture networks).

2. Model

In this section, we summarise the details of the model, which builds on that of Piegari et al. (2008, 2011). After describing the essential features of the Piegari et al. model — the fracture, magma movement and degassing algorithms — we move on to describe the crucial new feature introduced: the augmentation of the local stress in the vicinity of magma.

2.1. Earlier model: Piegari et al. (2008, 2011)

2.1.1. Fracture model

As introduced above, the CA model for volcanism is based on the OFC earthquake model (Olami et al., 1992), using it to simulate fractures in the country rock caused by volcanic tectonic activity. The OFC model defines a stress field $f_{i,j}$, on a 2D grid of size $L \times L$, with $1 \leq i \leq L$, $1 \leq j \leq L$. In the volcanic context, this corresponds to a vertical subsection beneath a volcano, with i labelling the vertical axis (with $i = L$ the row at the bottom of the grid), and j the horizontal axis. Each cell is initially assigned a random stress value $f_{i,j}$, uniformly distributed in the range $0 \leq f_{i,j} < 1$. In the homogeneous, isotropic case considered in earlier work, the stress at every cell is increased at constant strain rate ν . Evolving the system via time-steps of size Δt , the stress at each cell varies as $f_{i,j} \rightarrow f_{i,j} + \nu \Delta t$. This behaviour continues until the stress in any cell reaches the critical value, f_{crit} . This critical value is the same for all cells and, working with nondimensional variables, we can take $f_{\text{crit}} = 1$. When a cell reaches this threshold value it fractures: a proportion of the stress, determined by a model parameter ϵ , is distributed to the neighbouring cells, and the stress on the original cell is reduced to zero. Since each cell has a maximum of 4 neighbours (in the interior of the grid), the range $0 \leq \epsilon \leq 0.25$ is possible, with $\epsilon = 0.25$ corresponding to a conservative system. Following Piegari et al. (2011), we here consider a non-conservative system with $\epsilon = 0.2$. This redistribution of stress may cause the neighbouring cells to reach the critical value and fracture, resulting in further redistributions of stress; this process repeats, in an ‘avalanche’ effect, until the system is everywhere stable again (i.e. no cells remain with $f_{i,j} \geq f_{\text{crit}}$). These repeated stress relaxations are considered to occur instantaneously, before the next global strain increment, and constitute a single earthquake event. The net effect is to produce a network of fractured cells, involving between 1 and L^2 cells (with the latter, system-wide events being vanishingly rare), through which magma may move. The probability of fracture events involving N cells follows a power law in N , corresponding to the Gutenberg–Richter law.

Since the stress-loading process between fracture events is constant and homogeneous, the time until the next event can be calculated by observing the maximum value of $f_{i,j}$ after the preceding event. The next event will happen when the stress has increased by $\delta f = 1 - \max(f_{i,j})$. With a constant stress-rate ν , this will happen in time $\delta t = \delta f / \nu$. Rather than incrementing time in steps of Δt , we therefore step ahead to the next event by incrementing the time by δt , and increasing the stress on all cells by δf . This is equivalent to time-stepping in the limit $\Delta t \rightarrow 0$, but is computationally more efficient. We work with

non-dimensional time units, defined with respect to the stress-rate ν . In practice our calculations therefore use $\nu = 1$; if dimensional times are required, they could be calculated by multiplying our non-dimensional values by the time unit $\tau = f_{\text{crit}}/\nu$, where f_{crit} and ν are the physical values of interest.

The OFC model has been studied with various forms of boundary conditions at the edges of the grid. While this leads to quantitatively different results, the qualitative behaviour is unaffected. Here we use ‘rigid’ boundary conditions (as if the cells at the boundaries were connected to a rigid frame moving with the driving plate, within the slider-block model motivation for the OFC model). This is implemented using a grid of size $(L + 2) \times (L + 2)$, with the stress at the (‘dummy’) external cells ($i, j = 0, L + 1$) being reset to zero after each event. These conditions are non-conservative, with an additional loss of stress when boundary cells fracture: $\epsilon f_{i,j}/2$ at corner cells, $\epsilon f_{i,j}/4$ at other edge cells.

2.1.2. Magma movement

Piegari et al. (2008, 2011) developed the fracture model into a model for volcanism by adding a magma field $n_{i,j}$. In the original model (Piegari et al., 2008), $n_{i,j} = 0$ corresponds to no magma, while $n_{i,j} = 1$ indicates a magma filled cell. (A more refined model was introduced in Piegari et al. (2011); this is discussed in section 2.1.3.) All magma is assumed to originate from an unlimited reservoir (fed from a deeper supply), which is not modelled explicitly. The top of this magma reservoir occupies the central quarter of the external row below the grid, $i = L + 1$. Magma can enter the grid itself (the ‘magma chamber’) when any cell next to the reservoir becomes fractured as a result of the evolving stress field. Once inside the magma chamber, magma migrates through the fracture network towards the surface (which corresponds to the external row above our grid, $i = 0$). An eruption is said to occur once magma reaches a fractured cell adjacent to the surface (in row $i = 1$). While large avalanches of fracture events do occur, most fractures are localised small-scale events, during which batches of magma can only move relatively small distances through the chamber. The motion of magma through the system will therefore generally be rather gradual, taking the form of a ‘diffusive’ rise through the self-organised fracture network.

The detailed algorithms controlling the magma movement are explained in the flow diagrams in Figure 1. After each fracture event, the movement of magma from the reservoir to the chamber is considered first (panel a). Magma is then allowed to move through the fracture network (panel b). In implementing the magma movement algorithm, we repeatedly iterate over all cells within the grid: looping vertically down columns ($i = 1, \dots, L$) within a horizontal loop across rows ($j = 1, \dots, L$). The possibility of vertical movement due to buoyancy is considered throughout the grid before any horizontal movement is allowed. (Diagonal motion is not permitted.) We run this magma movement algorithm until no further vertical motion can take place, checking for eruptions (panel c) after each iteration of the algorithm. At this point, the current phase of magma movement is considered to be complete. The fractured cells close up, trapping any magma they contain, and the system evolves

in time to the next fracture event (following the rules of section 2.1.1).

Most eruptions only involve magma that has ascended through the magma chamber during multiple fracture events (and there are usually many fracture events between each eruption). However, a small number of larger, explosive eruptions can involve the reservoir directly; these would model events such as those at Soufrière Hills in Monserrat, considered by Scandone et al. (2009). In these unusual cases, where a fracture network directly connects the reservoir to the surface, the reservoir algorithm fills all such cells with magma, and the eruption algorithm immediately ejects this magma in an eruption. To avoid an infinite loop, only a single filling of the network from the reservoir takes place. Physically, the eruption is considered to have caused the collapse of the chamber walls surrounding the fracture network, preventing the rise of additional magma (e.g. Scandone et al., 2009). Note that such events would involve volatile-rich magma (see below) so will be particularly explosive.

2.1.3. Volatiles and Magma Degassing

In modelling volcanic explosivity, it is important to consider the volatile content of the magma, which can greatly affect the style of eruption. Piegari et al. (2011) introduced this concern, assuming that water is the dominant volatile element (although other volatiles might be treated similarly). In equilibrium, the dissolved water concentration, n_d , is determined by the lithostatic pressure p , as

$$n_d = 6.8 \times 10^{-8} p^{0.7}, \quad (1)$$

with n_d the fractional water content, and p the pressure in Pascal (Piegari et al., 2013), with the lithostatic pressure calculated as

$$p(z) = p_0 + g \int_0^z \rho(\zeta) d\zeta, \quad (2)$$

where $\rho(z)$ is the density of the rock at depth z , and $g = 9.81 \text{ ms}^{-2}$ is the gravitational acceleration. Thus the equilibrium value of n_d varies with depth, following the pressure variation. To replicate the model of Piegari et al. (2011), we adopt a grid of depth $h = 12 \text{ km}$, surface pressure $p_0 = 0$, and constant rock density $\rho(z) = \rho_0 = 2700 \text{ kgm}^{-3}$.

The dissolved water content at the depth of the reservoir, n_0 , is taken as $n_0 \approx 0.06$, or 6%. The gas lost due to exsolution, n_{loss} , is calculated as

$$n_{\text{loss}} = n_0 - n_d. \quad (3)$$

Thus moving from the reservoir to the surface (assuming local equilibration), n_d decreases from 0.06 to 0, and n_{loss} increases from 0 to 0.06. We follow Piegari et al. (2011) in considering as our magma field the quantity $n = (1 - n_{\text{loss}})$, which varies from 1 at the reservoir to 0.94 at the surface.

Water is exsolved (magma is equilibrated) if and only if the magma remains in the magma chamber between earthquake events, with $n_{i,j}$ then taking the value of $(1 - n_{\text{loss}})$ calculated for the depth at which the magma resides. This corresponds

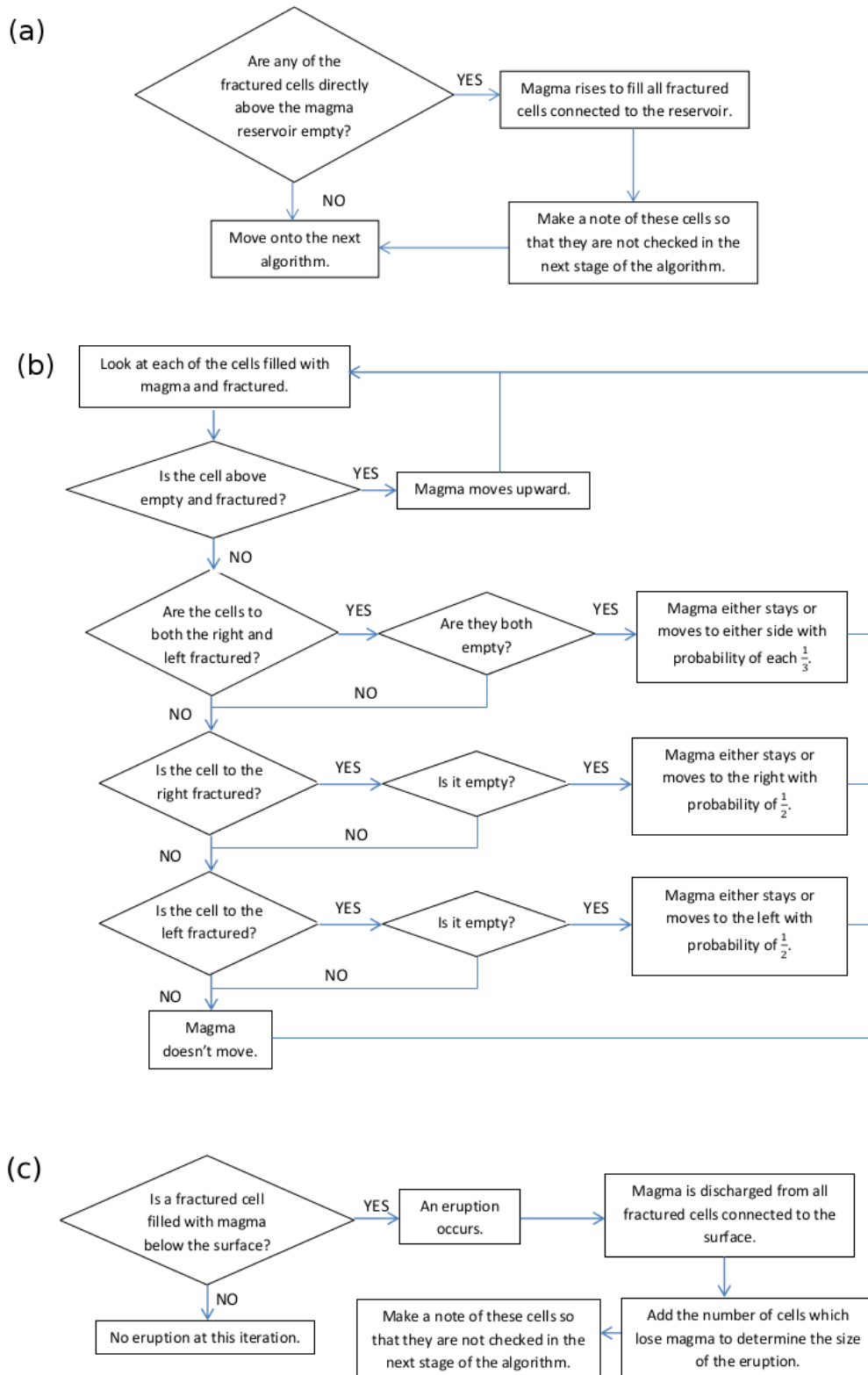


Figure 1: Flow diagrams describing: (a) the rise of magma from the reservoir into the chamber; (b) the movement of magma within the chamber; (c) eruptions from the magma chamber to the surface.

to ‘passive degassing’ (Newhall, 2007), with the volatiles escaping slowly through the surrounding country rock, and leaving the emplaced magma depleted in volatiles (and hence more viscous, less explosive), at the new equilibrium level. When magma migrates through the fracture network during a fracture event, it initially retains its volatile content. So when an eruption occurs, the magma reaching the surface will have a range of volatilities, reflecting the depths at which the various batches of magma last resided. Rarely, this will involve some saturated magma, which has ascended directly from the reservoir during that earthquake event. The mean volatility content of the magma taking part in an eruption is a proxy for the explosivity.

2.2. New model: magma-induced stress

In the earlier model described above, the stress field has been an independent quantity, entirely determined by the OFC model, without any feedback from the magma field. This models a uniform background rate of stress, without local variations. But as discussed in section 1, there are many reasons why magma intrusions should lead to enhanced local stress values. Here we adapt the OFC model to impose additional stress on cells containing magma.

To model an enhanced rate of stress in those cells as simply as possible, we increase the rate of stress in the magma-filled cells by a factor $(1 + \delta)$, where δ is a new model parameter. We therefore increase the local strain rate from ν to $\nu(1 + \delta)$. Since we have normalised time with respect to ν (see section 2.1.1), the stress in magma-filled cells will therefore increase by $(1 + \delta)\Delta t$ over a time interval Δt (during which time the stress in other cells will simply increase by Δt). To proceed directly to the next fracture event, as before, we need to consider the evolution of stress in cells with and without magma ($f_{i,j}^{\text{mag}}$ and $f_{i,j}^{\text{nomag}}$, respectively) separately. Note that $f_{i,j}^{\text{mag}}$ and $f_{i,j}^{\text{nomag}}$ are not parameterised in any way. They are simply the original stress field $f_{i,j}$, but now treated in one of two different ways, depending on whether or not cell (i, j) contains magma.

The time until the next fracture event in a cell without magma would be

$$\delta t_{\text{nomag}} = 1 - \max(f_{i,j}^{\text{nomag}}); \quad (4)$$

the time until the next fracture event in a cell containing magma would be

$$\delta t_{\text{mag}} = \frac{1 - \max(f_{i,j}^{\text{mag}})}{1 + \delta}. \quad (5)$$

The next event therefore occurs after the lesser of these two times,

$$\delta t = \min(\delta t_{\text{nomag}}, \delta t_{\text{mag}}), \quad (6)$$

and we can then update the stresses as

$$f_{i,j}^{\text{nomag}} \longrightarrow f_{i,j}^{\text{nomag}} + \delta t, \quad f_{i,j}^{\text{mag}} \longrightarrow f_{i,j}^{\text{mag}} + (1 + \delta) \delta t. \quad (7)$$

Note that the addition of magma-induced stress only directly affects the fracture model (the OFC model), which is now coupled to the magma model as described above; the algorithms for

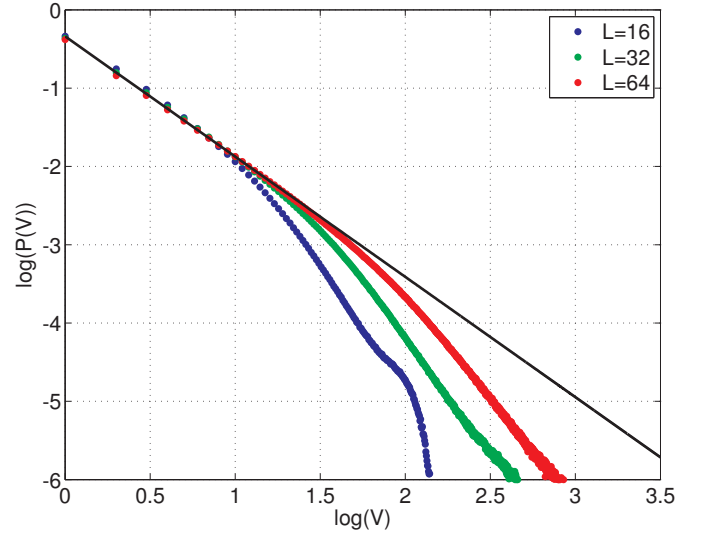


Figure 2: Probability distribution $P(V)$ of eruptions of size V , for varying L from runs with 10^8 eruptions. The straight line corresponds to the power law fit $P(V) = V^{-\alpha}$ with $\alpha \approx 1.49$.

magma movement and degassing remain unchanged. Nevertheless, the resulting eruption behaviour can differ markedly, in the presence of the different styles of fracture networks obtained in the coupled system. The fracture dynamics (and therefore also the eruption dynamics) of course depend on the value of our new parameter δ ; the outcome for varying values of δ is discussed in section 3.

2.3. Numerical Implementation

The model described above was implemented computationally in Fortran. Although some larger grid sizes were considered, we performed most runs on a grid of size $L = 64$. With the grid representing a length of 12 km in both directions, we therefore consider a cell spacing of 200 m. We typically perform runs involving 10^8 eruptions and analyse the statistics of the ensuing volcanic activity with respect to distributions of event size, repose time, and explosivity. For reasons of computational efficiency, the data for 10^8 eruptions are actually compiled from 40 individual runs, each of 2.5×10^6 eruptions. For each individual run, all data associated with the first 10^5 eruptions were discarded, with the consequence that all data analysed are from systems that have attained statistically steady states.

3. Results

3.1. Earlier model: Piegari et al. (2008, 2011)

Before investigating the detailed effects of the new magma-induced stress mechanism described in section 2.2, we reproduce the behaviour described by Piegari et al. (2008, 2011) for their model (corresponding to our case $\delta = 0$). We had previously verified our implementation of the underlying OFC model with the results of Olami et al. (1992).

Figure 2 shows the probability density $P(V)$ of eruptions of size V (i.e. the number of cells with magma involved in the

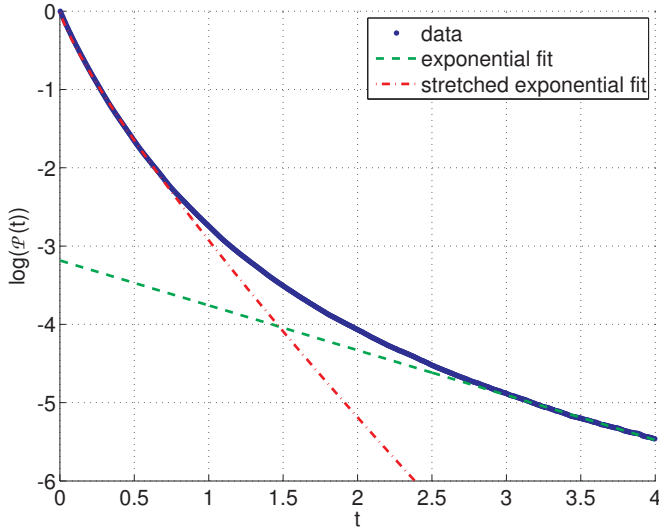


Figure 3: Cumulative probability distribution $\mathcal{P}(t)$ of inter-eruption times (blue dots), calculated for 10^8 events with $L = 64$. An exponential fit to data in the last quarter of this range (red line), and a stretched exponential fit to data in the first quarter of this range (magenta line) are also shown.

eruption), on a log-log scale, from runs involving 10^8 eruptions in systems of varying size L . (We use \log_{10} throughout.) The straight line fit reflects a power law behaviour, $P(V) \propto V^{-\alpha}$, mirroring the observed fit to VEI values of Simkin (1993). The power law behaviour breaks down at larger event sizes, with the point of divergence being somewhat dependent upon the system size (because the larger events are not possible within smaller systems). Figure 2 should be compared with Figure 2 of Piegari et al. (2008). They quote a value $\alpha = 1.6$ for their power law exponent, but inspection of their figure suggests a value closer to 1.4. Our straight line fit, calculated for the range $0 \leq \log V \leq 1$, corresponds to an exponent of 1.49. Given the uncertainties in the fit (the fit varies slightly with the range over which it is calculated, as well as having a formal uncertainty) and the possibility of minor differences between the fine details of our magma movement algorithms, we consider this agreement acceptable.

Figure 3 is a log-linear plot of the cumulative probability $\mathcal{P}(t)$, more formally $\mathcal{P}(T \geq t)$, of inter-eruption intervals (repose times) of duration T , for the same model as above. Note that this is the complement of the more conventional cumulative probability $\bar{\mathcal{P}}(T \leq t)$, related by $\mathcal{P}(T \geq t) = 1 - \bar{\mathcal{P}}(T \leq t)$; thus $\mathcal{P}(0) = 1$ and $\mathcal{P}(t) \rightarrow 0$ as $t \rightarrow \infty$. This can be compared to Figure 3 of Piegari et al. (2008). In both cases the time units are non-dimensional (see section 2.1.2), and the plots exclude the longest repose times, in the tail of the distribution.

For large repose times (i.e. for $3 \leq t \leq 4$) the $\mathcal{P}(t)$ curve in Figure 3 approaches a linear slope, corresponding to exponential behaviour, $\mathcal{P}(t) \propto \exp(-t/\tau_1)$. Here $\tau_1 \approx 0.76 \pm 0.06$, with the uncertainty in the fit corresponding to variations due to different choices of range. Exponential behaviour of this type is the expected result for a Poisson process, indicating that such events are ‘memoryless’ (i.e. independent of previous similar events). This exponential behaviour only occurs for

the long repose-time events towards the tail of the distribution (accounting for less than 0.1% of the total events). The majority of eruptive events have a much shorter repose time. For such smaller repose-time events, the data is better approximated by a stretched exponential fit of the form $\mathcal{P}(t) \propto \exp(-(t/\tau_0)^\beta)$, where $\beta \approx 0.83$ and $\tau_0 \approx 0.10$. (The smaller events are therefore not well modelled as a Poisson process. This is reasonable for the model of volcanism considered here, with magma moving through the systems in small batches, and consecutive events being linked via the dynamics of magma transport; we do not expect memoryless behaviour for such events.) These results are qualitatively similar to those reported by Piegari et al. (2008). However, there is some uncertainty in how their timescale relates to ours: Piegari et al. (2008) report their timescale in units of ν^{-1} (and state that their results depend on ν), whereas we have scaled ν out of our calculations. A factor of 10^4 difference in the respective timescales would account for differences between the reported fitting parameters. In any event, our agreement with Piegari et al. is qualitatively satisfactory, even if the quantitative comparison remains unclear.

The behaviour of volatile components within the model (and the associated range of explosivities of the eruptions) can also be compared with the calculations of Piegari et al. (2011). Figure 4 shows a histogram of the probability density $P(n_{\text{loss}})$ of events with mean gas-loss n_{loss} , on a log-linear scale. The eruption statistics were obtained using a bin width of 0.2% in n_{loss} . The histogram, which is in broad agreement with Figure 4 of Piegari et al. (2011), shows the far greater probability of eruptions involving magma that has lost most of its gas content (having degassed relatively close to the surface). At the other end of the spectrum, eruptions involving almost fully saturated magma are extremely rare. Such eruptions, with significant amounts of magma erupting directly from the reservoir (or at least from locations near the base of the magma chamber) are typically larger in size, and more explosive. The distribution is approximately exponential for most events, showing a (broadly) linear trend on the log-linear plot.

3.2. New model: magma-induced stress

We now consider the new effect of magma-induced stress ($\delta > 0$). Figure 5 shows the probability density functions $P(V)$ for various δ in the range 0.1–0.6, from simulations with $L = 64$ involving 10^8 eruptions. These can be compared with the corresponding distribution for $\delta = 0$, also shown on each panel. The new functions $P(V)$ continue to show a power law distribution for smaller events, but the range over which this applies depends on δ ; it decreases from $\log V \approx 1.5$ with $\delta = 0$, to $\log V \approx 1.1$ with $\delta = 0.6$. For intermediate δ ($0.1 \leq \delta \leq 0.4$), there is a local peak of events of moderate size ($\log V \approx 1.5$) and, after a relative dearth of intermediate size events, there is another prominent peak of large events at $\log V \approx 3.0$ – 3.25 . Note that for intermediate values of δ , both these peaks lie above the continuation of the power law line; so, although obviously rarer than small events, these eruptions must be considered relatively frequent. It is possible that the extent of the peak at large V is somewhat limited by the relatively small L employed here, and future calculations will investigate this.

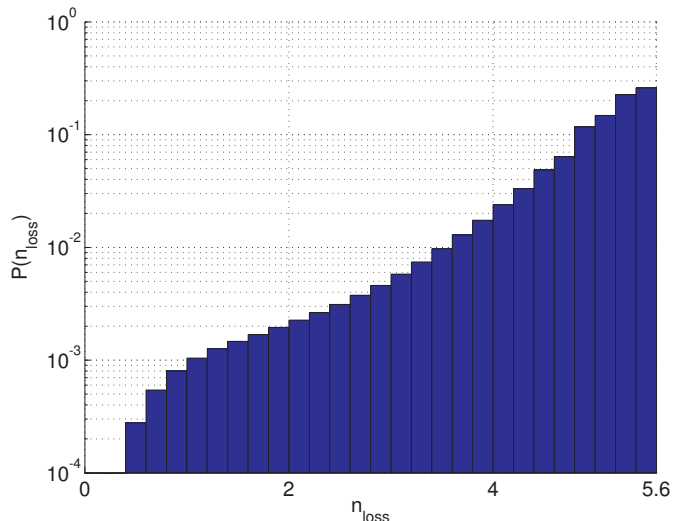


Figure 4: Probability distribution $P(n_{\text{loss}})$ of eruptions with percentage of gas loss n_{loss} , calculated for 10^8 events with $L = 64$.

The variation with δ of the mean eruption size \bar{V} , and the slope and intercept of the power law fits, are given in Table 1. The behaviour with increasing δ is clear. As δ increases to 0.2, the mean eruption size \bar{V} increases significantly. Note that this coincides with a steepening of the power law slope, so this effect is clearly due to the localised peaks in the $P(V)$ distribution. As δ increases further, these trends reverse; the intermediate and large event size peaks become less significant, and the main effect of the magma-induced stress now seems to be an increased dominance of smaller events. These effects are due to the relative ease with which the system allows magma to migrate between the reservoir and the surface, with increasing δ ; this is discussed further below, after additional aspects of the behaviour with varying δ have been discussed.

The effects on the cumulative probability distribution of events $\mathcal{P}(t)$, are consistent with the picture described above; Figure 6 shows this distribution for the same values of δ considered above. (The corresponding distribution for $\delta = 0$ is shown in Figure 3.) The variation with δ of the mean inter-eruption time and the parameters of the stretched exponential and exponential fits are also given in Table 1. As δ increases to 0.1, the mean inter-eruption time \bar{T} increases, due to the increasing prominence of intermediate and large eruptions (which empty the central region of the magma chamber, leading to significant times before subsequent eruptions). The timescale τ_1 for long inter-eruption times (from the exponential fit) increases from 0.76 to 0.84. For small inter-eruption times, τ_0 also increases (from 0.10 to 0.13) and the stretching exponent β decreases slightly (from 0.83 to 0.79). As δ increases further however, these trends again reverse — for $\delta \approx 0.3$ –0.4, the $P(t)$ distribution is broadly similar to that for $\delta = 0.0$ — and by $\delta = 0.6$, the shorter inter-eruption times (predominantly associated with smaller eruptions) increasingly dominate the $P(t)$ distribution, with very long inter-eruption times increasingly rare.

Histograms of the probability density $P(n_{\text{loss}})$ of events with mean gas-loss n_{loss} , for varying δ , are shown in Figure 7. Com-

pared to the case $\delta = 0$ shown in Figure 4, for $\delta = 0.1$ the exponential relationship (i.e. the straight line section on the log-linear plot) is now restricted to $n_{\text{loss}} \gtrsim 3.5\%$. For smaller n_{loss} , the probability density function is now much flatter; i.e. high explosivity events with small gas loss are now more common. For intermediate δ ($\delta \approx 0.2$), a pronounced peak develops at $n_{\text{loss}} \approx 0$ (i.e. the most explosive events are now comparatively common). For higher δ ($\delta > 0.2$), while this peak of ultra-explosive events remains relatively prominent, the probability of explosive events more generally decreases again.

Once magma has moved into a fractured cell and the stress level is reset to zero, that batch of magma must wait for the cell to fracture again before being able to move onwards towards an eruption. If this process takes a particular time on average, in the earlier model ($\delta = 0$), then that time will decrease in the new model, by an amount depending upon δ . Note that there is a nonlinear effect at work here. The more cells contain magma, the greater the net strain rate, and the more frequent the occurrence of fracture events; the more frequent the occurrence of fracture events, the more magma is able to enter the system. This magma does not reside in the system for as long however; the increased seismicity allows the magma to be transported more efficiently through the system. This mechanism also contributes to the increased likelihood of large eruptions. Since clusters of cells containing magma all have the increased strain rate, they are all more likely to be involved in further fracture events, one of which may ultimately cause an eruption.

Note that the nonlinear nature of the link between magma and stress fields, and the dependence of the behaviour on the statistical distributions of both these fields, means that there is not a critical value of δ at which the statistical behaviour of the system changes (and which would therefore clearly mark different regimes). Rather, as is clear from Table 1, the effects of increasing δ can act in differing ways, resulting in non-monotonic behaviour, and in different measures achieving extreme values at different values of δ . Nevertheless, the behaviour with increasing δ can be understood in terms of the dynamics of magma movement with the model, as discussed below.

To clarify the dynamics for $\delta > 0$, we have analysed the frequency of occurrence of events within each cell. Figure 8 shows the frequency distribution of fracture events for $\delta = 0$ and $\delta = 0.4$. With $\delta = 0$ the distribution is homogeneous, except for a decrease in the number of events near the edges of the grid, where the effect of the boundaries leads to cells receiving less stress via redistributions from events at neighbouring cells. This homogeneity is to be expected, given the constant applied stress, and lack of feedback from magma occupation. In contrast, with $\delta > 0$, fracture events become increasingly concentrated in the lower central section of the grid, immediately above the magma reservoir. Again, this should be expected, since the mechanism for magma entering the chamber requires magma to travel through this part of the grid; and since magma occupation now leads to increased strain rates, this must ultimately lead to more fracture events there. (Although not shown here, the frequency distribution of magma occupation supports this conclusion.) In physical terms, the country rock in this region is repeatedly failing under the net increased stress, and so

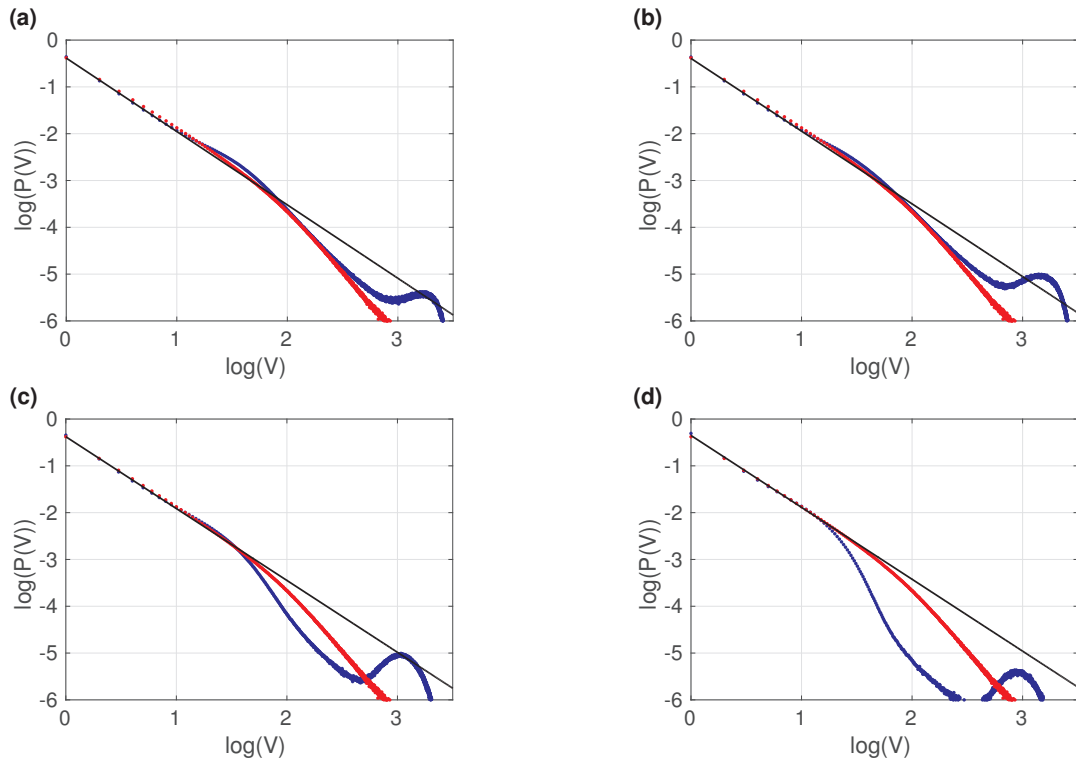


Figure 5: Probability distribution $P(V)$ for eruptions of size V , using data from 10^8 eruptions with $L = 64$ for varying δ (in blue): (a) $\delta = 0.1$; (b) $\delta = 0.2$; (c) $\delta = 0.4$; (d) $\delta = 0.6$. The straight lines are the power law fits described in Table 1. The red data show the corresponding distribution for $\delta = 0$, as shown in Figure 2.

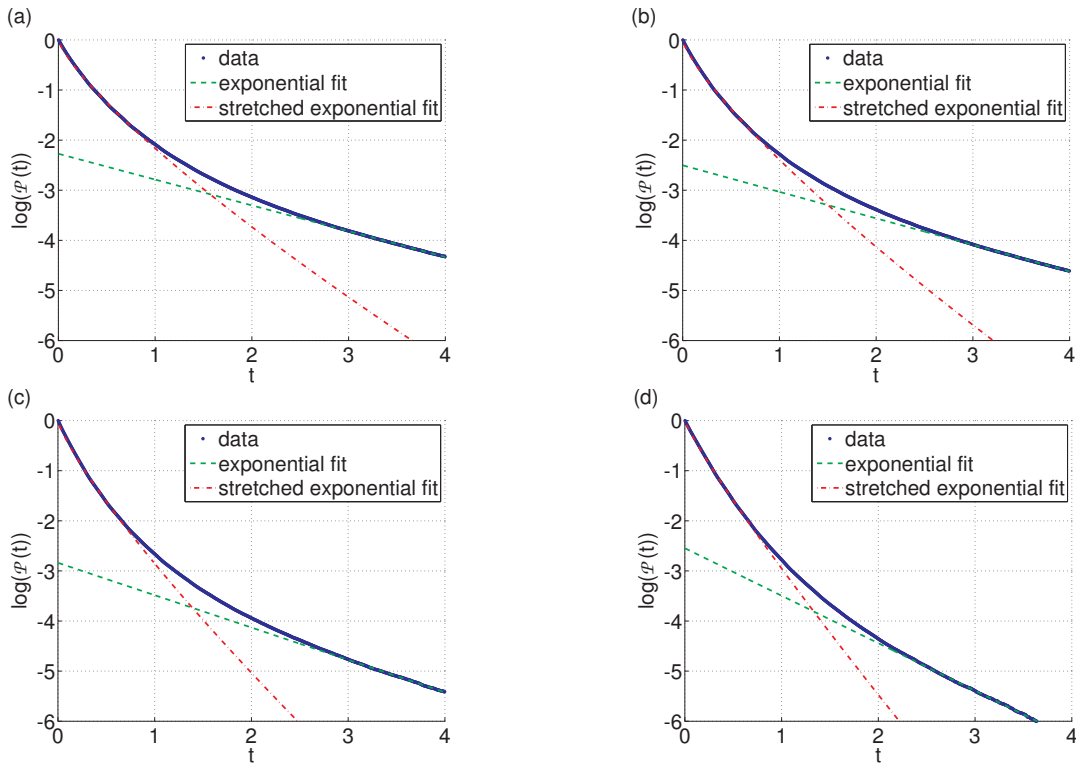


Figure 6: Cumulative probability distribution $\mathcal{P}(t)$ of inter-eruption times, using data from 10^8 eruptions with $L = 64$ for varying δ : (a) $\delta = 0.1$; (b) $\delta = 0.2$; (c) $\delta = 0.4$; (d) $\delta = 0.6$. The exponential and stretched exponential fits are described in Table 1.

δ	0.0	0.1	0.2	0.3	0.4	0.5	0.6
\bar{V}	9.80	19.5	28.5	22.8	16.3	11.2	7.01
α	1.49	1.57	1.55	1.54	1.54	1.53	1.54
$P(V = 1)$	-0.384	-0.385	-0.392	-0.385	-0.378	-0.367	-0.351
\bar{T}	0.115	0.157	0.140	0.124	0.119	0.120	0.127
τ_0	0.10	0.13	0.12	0.10	0.10	0.10	0.12
β	0.83	0.79	0.79	0.80	0.82	0.85	0.89
τ_1	0.76	0.84	0.82	0.77	0.67	0.53	0.46

Table 1: Some eruptions statistics with varying δ . Mean eruption size \bar{V} , and the slope ($-\alpha$) and intercept ($P(V = 1)$) from the power law fits in Figures 2, 5. Mean inter-eruption time \bar{T} , and stretched exponential (τ_0, β) and exponential (τ_1) parameters from the fits in Figures 3, 6.

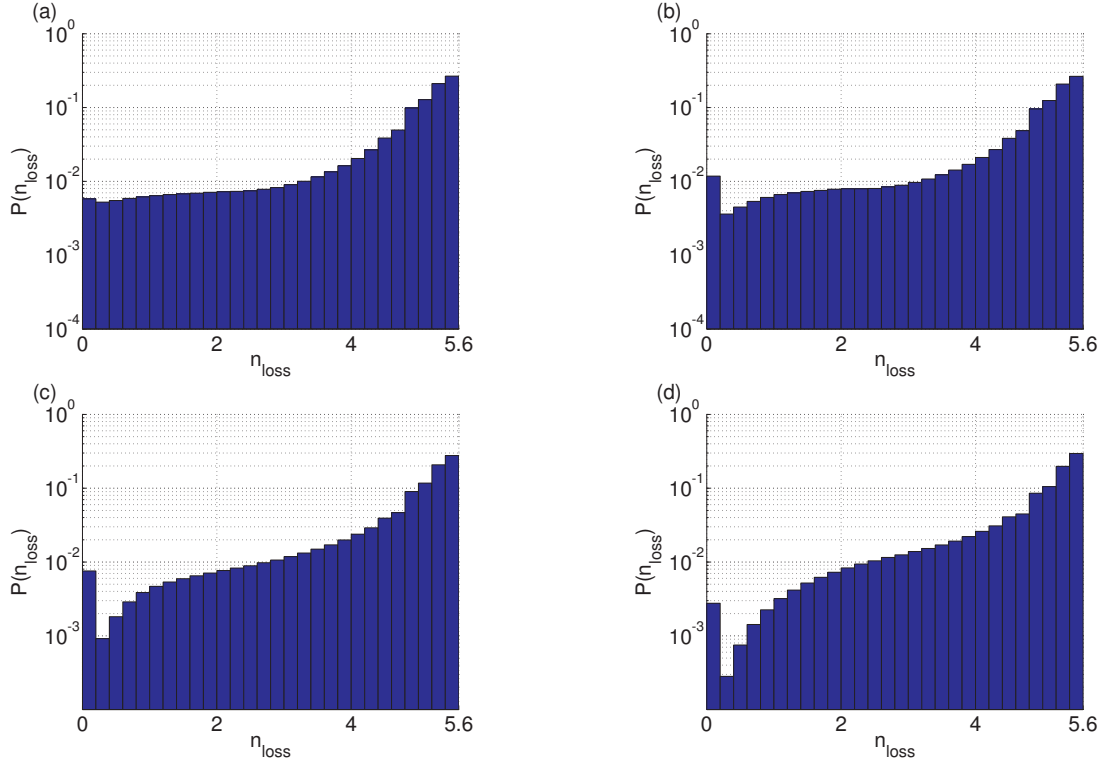


Figure 7: Probability distribution $P(n_{\text{loss}})$ of eruptions with percentage of gas loss n_{loss} , using data from 10^8 eruptions with $L = 64$ for varying δ : (a) $\delta = 0.1$; (b) $\delta = 0.2$; (c) $\delta = 0.4$; (d) $\delta = 0.6$.

is experiencing static fatigue. The part of the grid experiencing repeated failures will clearly depend on the width of the opening connecting the magma chamber to the reservoir (here the central quarter of the grid). Piegari et al. (2011) stated that the width of the reservoir opening did not alter the statistical properties of the earlier model, but the addition of magma-induced stress might well change this conclusion. This has not yet been explored.

The frequency distribution of cells involved in eruptions is shown in Figure 9. From the panels with $\delta > 0$, it is clear that cells at greater depths take part in eruptions more frequently than for $\delta = 0$. This is particularly the case within a central column above the opening to the magma reservoir. The appearance of this central column is a clear signature of the presence of magma-induced stresses. Eruptions involving deep-lying magma include those large eruptions causing the large- V peak in the $P(V)$ distribution noted above, but also smaller, volatile-

rich (low n_{loss} , explosive) eruptions. In contrast, when $\delta = 0$, the cells involved in eruptions more frequently come from only the upper regions of the grid, and so eruptions more often contain less volatiles (so are more effusive). For larger δ ($\delta \gtrsim 0.4$), the effectiveness of the magma-induced stress in assisting the vertical transport of magma through the central conduit is such that the preference towards large, highly-explosive eruptions reverses, and smaller, shallower events again become relatively more likely. This is because magma batches can now ascend more ‘continuously’; i.e. via more frequent small steps. This explains the reduction of the large- V peak in the $P(V)$ distribution, observed for $\delta \gtrsim 0.2$ in Figure 5.

With regards to Figure 9, it may be worth noting two minor artefacts in the distributions of near-surface eruptions that arise due to our CA model. There are local peaks in the eruption frequency near the edges of our domain, due to the finite width of our magma chamber. (This is most pronounced for

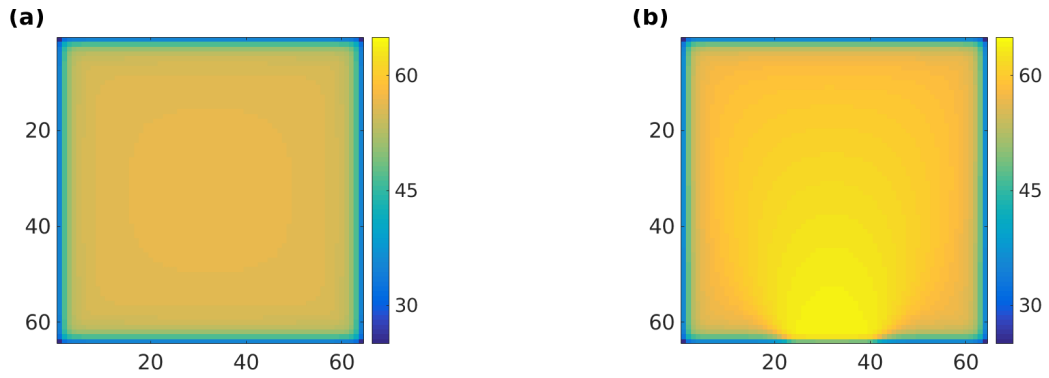


Figure 8: Frequency distributions of cells involved in fractures, for: (a) $\delta = 0$; (b) $\delta = 0.4$. The numbers on the colour bar correspond to millions of fracture occurrences, from a simulation with $L = 64$ and 10^8 eruptions.

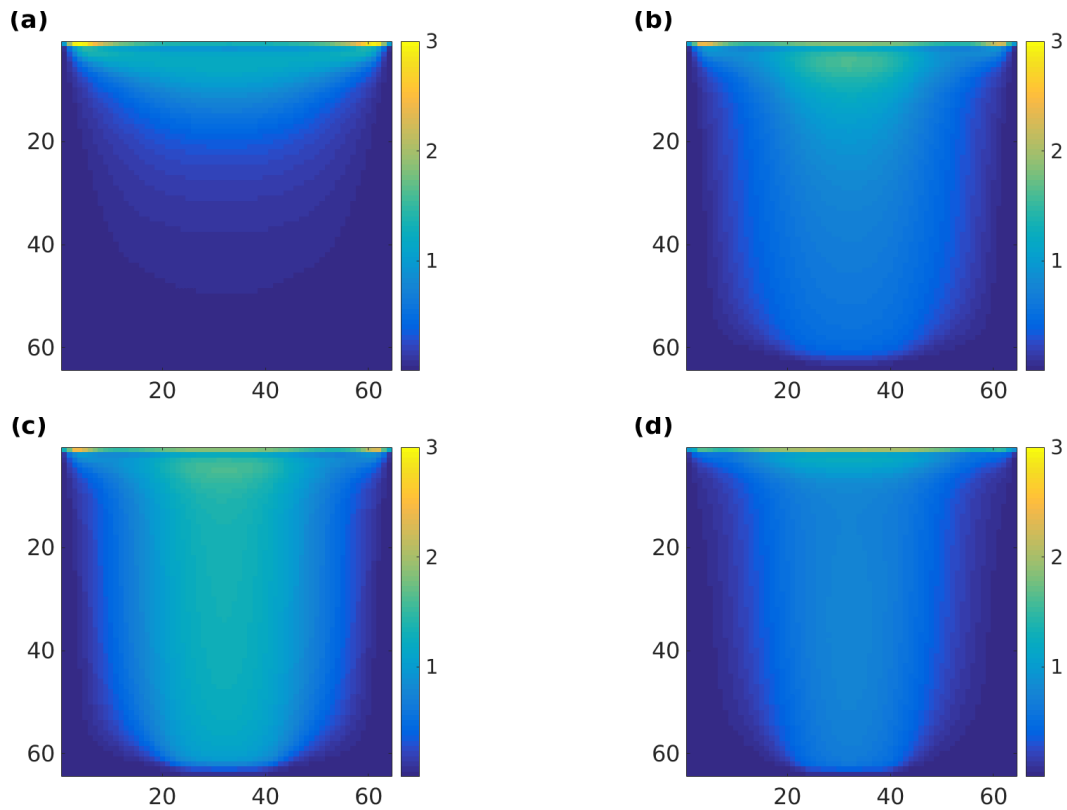


Figure 9: Frequency distributions of cells involved in eruptions, for: (a) $\delta = 0$; (b) $\delta = 0.1$; (c) $\delta = 0.2$; (d) $\delta = 0.4$. The numbers on the colour bar correspond to millions of eruption occurrences, from a simulation with $L = 64$ and 10^8 eruptions.

$\delta = 0$, but persists also for $\delta > 0$.) A wider domain would smooth out this feature. There is also a local minimum in the eruption frequency in row 2, due to a combination of the edge effect in the fracture distribution (shown in Figure 8) and our magma movement and eruption algorithms. We do not think these phenomena affect our overall eruption statistics.

To summarise, the addition of magma-induced stress has allowed for volcanic activity involving relatively more frequent large, explosive events. Within the fracture-network model of magma batch migration, this is therefore closer to a more continuous central conduit model, in which magma does not move too far horizontally away from the region above magma reservoir. Within the classification of Scandone et al. (2009), the eruptions are moving towards a more sustained style. It is important to appreciate that this feature has not been imposed (along the lines of Piegari et al., 2012, 2013, who adapted their magma movement algorithm to enforce axial symmetry). Instead it arises naturally from the increase in stress in regions containing magma. In the VEI index, 61% of volcanoes feature central craters (Simkin, 1993), so the model is arguably now more suited to modelling the majority of volcanoes.

4. Discussion

We have adopted the model of Piegari et al. (2008, 2011) as the basis for our study, replicating their essential results: a power law relation between eruption size and frequency; a stretched exponential distribution of repose times between events, approaching a pure exponential distribution only for the longest repose times; and a broadly exponential distribution of eruption volatilities. This model was then extended to include feedback from the magma upon the fracture network, via a local magma-related augmentation of the stress field. This has the effect of creating new peaks in the probability distribution $P(V)$, corresponding to relatively more frequent intermediate and large events, with the range of power law behaviour being restricted to smaller events. The mean eruption size consequently increases, with associated increases in the mean inter-eruption time and the likelihood of high explosivity eruptions.

Our new model effectively favours a central ‘axial’ conduit, as found in many volcano systems (and which otherwise must be artificially imposed, as in Piegari et al., 2012). In this context, it is worth noting that Pinel and Jaupart (2003) find that the increased stress in the upper crust from the weight of edifice volcanoes (e.g. stratovolcanoes) is comparable to tectonic stresses and overpressures within magma cavities. Furthermore the highest stress is distributed in such a way that it favours the formation of a central conduit system. Insofar as our magma-induced stress also leads to such centralisation, it might be argued that we are modelling this edifice effect by proxy.

There are many additions that might be made to our model. For example, we have not explored the possibility of including a low density surface layer, which would lead to the creation of near-surface dikes and sills, and in the process act as a ‘cap’ on the eruption process (Piegari et al., 2012, 2013). Such a cap leads to a new peak in the probability of long repose time events (on a characteristic timescale controlled by the width of

the low density surface layer), and also leads to fewer ‘explosive’ (high volatile content) events. Given that more explosive events tend to be favoured in our magma-induced stress model, it would be interesting to see how these two effects would interact. We might also consider moving to a 3D model, or perhaps implementing heterogeneous or anisotropic variants of the OFC model for the underlying stress field, to reflect the vertical orientation (with strong pressure gradient) required in the current context. In the existing model, the timescale of magma movement is clearly separated from that of stress-field evolution (the former being effectively instantaneous on the timescale of the latter). We might consider adapting the model to deal with the two timescales in a more continuous way.

While we would argue that we have modelled the local stress enhancement due to the magma in a very natural way (at least within the idealised spirit of the model), there are possible modifications that could be made. For example, we might choose to increase the local stress only around magma batches that moved during the most recent fracture. Alternatively, we might apply some magma-induced stress in cells surrounding those containing magma batches (out to some specified distance), as well as in the magma cells themselves. We could also associate a local stress increase with the occurrence of passive degassing (making the stress proportional to the extent of degassing), to model the occurrence of shallow (long period) earthquakes caused by this process.

The addition of magma-induced stress to the CA model opens up new possibilities for studying different styles of volcanism and volcanic-related seismic activity. With or without the possible modifications described above, there is much to be gained from comparing our results with those of different models, as well as with real observations. Sachs et al. (2012) consider the possible deviations from power law statistics for earthquakes and volcanoes, and for SOC models of these, focusing on extreme size events that occur more often than extrapolations would suggest (so called ‘dragon-kings’). In those terms, the peak of large events obtained for $\delta > 0$ in our model might be considered dragon-kings. There are other statistical comparisons that could also be carried out. For example, Watt et al. (2007) considered statistical fits to sequences of Vulcanian explosions, finding support for Weibull and log-logistic fits. Connor et al. (2003) had previously modelled such a sequence from Soufrière Hills via a log-logistic distribution, arguing that the log-logistic distribution arises from competing physical processes of gas bubble pressurisation and vesiculation associated with the magma movement.

More detailed study of the statistics of variant CA systems — incorporating the differing forms of feedback from magma to stress fields discussed above (i.e. differing forms of local stress enhancement) — would allow us to investigate the mechanisms behind such statistical distributions. The present work constitutes a first step in this direction.

Acknowledgements

We thank Ester Piegari for helpful discussions concerning her calculations, and thank the reviewers and editor for their com-

ments, which helped us to clarify a number of points.

Bibliography

References

- Bak, P., Tang, C., 1989. Earthquakes as a self-organized critical phenomenon. *Journal of Geophysical Research* 94 (B11), 15635–15637.
- Bak, P., Tang, C., Wiesenfeld, K., 1988. Self-organized criticality. *Physical Review A* 38 (1), 364–374.
- Burridge, R., Knopoff, L., 1967. Model and theoretical seismicity. *Bulletin of the Seismological Society of America* 57, 341–371.
- Connor, C. B., Sparks, R. S. J., Mason, R. M., Bonadonna, C., Young, S. R., Jul. 2003. Exploring links between physical and probabilistic models of volcanic eruptions: The Soufrière Hills Volcano, Montserrat. *Geophysical Research Letters* 30 (13), 1701.
- Emerman, S., Turcotte, D., Spence, D., 1986. Transport of magma and hydrothermal solutions by laminar and turbulent fluid fracture. *Physics of the Earth and Planetary Interiors* 41 (4), 249–259.
- Gonnermann, H., Manga, M., 2003. Explosive volcanism may not be an inevitable consequence of magma fragmentation. *Nature* 426 (6965), 432–435.
- Gutenberg, B., Richter, C. F., 1956. Magnitude and energy of earthquakes. *Annali di Geofisica* 9, 1–15.
- Jensen, H. J., 1998. *Self-Organized Criticality*. Cambridge University Press, Cambridge.
- Kilburn, C. R. J., Voight, B., 1998. Slow rock fracture as eruption precursor at Soufriere Hills Volcano, Montserrat. *Geophysical Research Letters* 25 (19), 3665–3668.
- Lachowycz, S. M., Pyle, D. M., Mather, T. A., Varley, N. R., Odbert, H. M., Cole, P. D., Reyes-Dvila, G. A., 2013. Long-range correlations identified in time-series of volcano seismicity during dome-forming eruptions using detrended fluctuation analysis. *Journal of Volcanology and Geothermal Research* 264, 197–209.
- Lister, J., Kerr, R., 1991. Fluid-mechanical models of crack-propagation and their application to magma transport in dykes. *Journal of Geophysical Research* 96 (B6), 10049–10077.
- Neuberg, J., 2000. Characteristics and causes of shallow seismicity in andesite volcanoes. *Philosophical Transactions of the Royal Society of London A* 358 (1770), 1533–1546.
- Newhall, C., Self, S., 1982. The Volcanic Explosivity Index (VEI) - an estimate of explosive magnitude for historical volcanism. *Journal of Geophysical Research* 87 (C2), 1231–1238.
- Newhall, C. G., 2007. Volcanology 101 for Seismologists. In: Kanamori, H. (Ed.), *Treatise on Geophysics, Volume 4: Earthquake Seismology*. Elsevier, Amsterdam, pp. 351–388.
- Olami, Z., Feder, H. J. S., Christensen, K., Feb 1992. Self-organized criticality in a continuous, nonconservative cellular automaton modeling earthquakes. *Phys. Rev. Lett.* 68, 1244–1247.
- Piegari, E., Cataudella, V., Di Maio, R., Milano, L., Nicodemi, M., Scandone, R., 2008. A model of volcanic transport by fracturing stress mechanisms. *Geophys. Res. Lett.* 35, L06308.
- Piegari, E., Di Maio, R., Scandone, R., Milano, L., Apr. 2011. A cellular automaton model for magma ascent: Degassing and styles of volcanic eruptions. *Journal of Volcanology and Geothermal Research* 202, 22–28.
- Piegari, E., Maio, R. D., Scandone, R., 2012. Effects of different rock density profiles on magma ascent and on the statistical distributions of simulated eruptions. *Bollettino di Geofisica Teorica ed Applicata* 53 (4), 551–558.
- Piegari, E., Maio, R. D., Scandone, R., 2013. Analysis of the activity pattern of volcanoes through self-organized crack networks: The effect of density barriers – An application to Vesuvius activity in the period 1631–1944. *Earth and Planetary Science Letters* 371–372, 269–277.
- Pinel, V., Jaupart, C., 2003. Magma chamber behavior beneath a volcanic edifice. *Journal of Geophysical Research* 108 (B2), 2072.
URL <http://dx.doi.org/10.1029/2002JB001751>
- Sachs, M., Yoder, M., Turcotte, D., Rundle, J., Malamud, B., 2012. Black swans, power laws, and dragon-kings: Earthquakes, volcanic eruptions, landslides, wildfires, floods, and soc models. *The European Physical Journal Special Topics* 205 (1), 167–182.
- Scandone, R., Cashman, K. V., Malone, S. D., Jan. 2007. Magma supply, magma ascent and the style of volcanic eruptions. *Earth and Planetary Science Letters* 253, 513–529.
- Scandone, R., Giacomelli, L., Speranza, F. F., Plastino, W., 2009. Classification and quantification of volcanic eruptions. *Bollettino di Geofisica Teorica ed Applicata* 50 (2), 103–116.
- Shaw, H. R., Chouet, B., 1991. Fractal hierarchies of magma transport in hawaii and critical self-organization of tremor. *Journal of Geophysical Research* 96 (B6), 10191–10207.
- Siebert, L., Simkin, T., Kimberley, P., 2010. *Volcanoes of the World*. Smithsonian Institution; University of California Press, Berkeley and Los Angeles.
- Simkin, T., 1993. Terrestrial volcanism in space and time. *Annual Review of Earth and Planetary Sciences* 21, 427–452.
- Turcotte, D. L., 1997. *Fractals and chaos in geology and geophysics*. Cambridge University Press, Cambridge.
- Watt, S. F. L., Mather, T. A., Pyle, D. M., Sep. 2007. Vulcanian explosion cycles: Patterns and predictability. *Geology* 35, 839.